

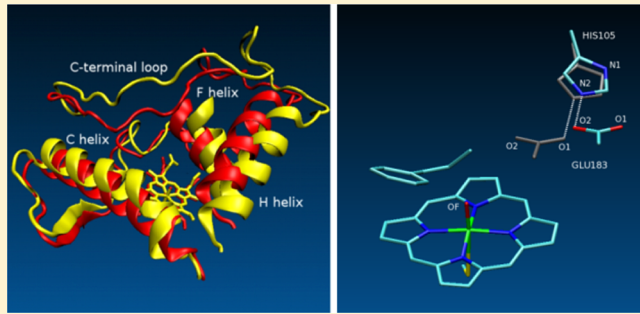
Chloroperoxidase-Catalyzed Epoxidation of *cis*- β -Methylstyrene: Distal Pocket Flexibility Tunes Catalytic Reactivity

Alexander N. Morozov* and David C. Chatfield*

Department of Chemistry and Biochemistry, Florida International University, 11200 SW Eighth Street, Miami, Florida 33199, United States

S Supporting Information

ABSTRACT: Chloroperoxidase, the most versatile heme protein, has a hybrid active site pocket that shares structural features with peroxidases and cytochrome P450s. The simulation studies presented here show that the enzyme possesses a remarkable ability to efficiently utilize its hybrid structure, assuming structurally different peroxidase-like and P450-like distal pocket faces and thereby enhancing the inherent catalytic capability of the active center. We find that, during epoxidation of *cis*- β -methylstyrene (CBMS), the native peroxidase-like aspect of the distal pocket is diminished as the polar Glu183 side chain is displaced away from the active center and the distal pocket takes on a more hydrophobic, P450-like, aspect. The P450-like distal pocket provides a significant enthalpic stabilization of ~ 4 kcal/mol of the 14 kcal/mol reaction barrier for gas-phase epoxidation of CMBS by an oxyferryl heme-thiolate species. This stabilization comes from breathing of the distal pocket. As until recently the active site of chloroperoxidase was postulated to be inflexible, these results suggest a new conceptual understanding of the enzyme's versatility: catalytic reactivity is tuned by flexibility of the distal pocket.



I. INTRODUCTION

Chloroperoxidase (CPO), a heme-thiolate protein secreted by the marine fungus *Caldariomyces fumago*, has received much attention as the most versatile known heme enzyme. The signature function of CPO is to catalyze halogenation of electron-rich organic substrates.^{1–4} The catalytic cycle begins with a peroxide-like two-electron oxidation of the native enzyme, using hydrogen peroxide or other suitable peroxide, to form a highly reactive oxyferryl porphyrin π -cation radical intermediate known as Compound I.^{5,6} Hereafter, we use CPO-I when referring to the Compound I form of CPO in particular and Cpd I when referring to Compound I in general. This initial reaction is followed by oxidation of a substrate, and the catalytic cycle ends as CPO regains the native state. The halogenation function of CPO is accompanied by a variety of promiscuous catalytic activities,⁷ including reactions characteristic of peroxidase, catalase, and cytochrome P450 (P450). Such versatile catalytic activity makes CPO a promising target for rational bioengineering.⁸

Since its discovery in the early 1960s,⁹ CPO has been the subject of continuous, intense research¹⁰ aimed at understanding the remarkable versatility of its catalytic properties. An X-ray crystallographic study¹¹ revealed that the active site of CPO has a hybrid peroxidase-P450 structure (Figure 1). Like P450, the proximal pocket of CPO's active site possesses a cysteine-derived thiolate ligand to the heme iron.¹¹ It is generally accepted that a proximal ligand plays an important role in controlling the redox potential and stability of the Cpd I

form of heme enzymes.¹² For P450 it has also been postulated that a thiolate ligand facilitates Cpd I formation by serving as a strong electron donor to promote O–O bond cleavage.¹³ For CPO, however, the effect of replacement of the proximal cysteine ligand by a histidine resulted only in a minor decrease of the reactivity while the versatility of the catalytic function remained intact.¹⁴ For this reason it was suggested that the distal pocket residues are mainly responsible for the versatility of the catalytic function of CPO.¹⁴

The distal pocket of CPO resembles that of peroxidases more than that of P450s. Whereas P450s possess a hydrophobic distal pocket, in CPO and peroxidases, the distal pocket has a polar character due to the presence of a residue with general acid–base properties, which facilitates formation of Cpd I.¹¹ Most traditional heme peroxidases use a histidine for this purpose, but CPO uses a glutamic acid (Glu183).^{11,15} For glutamic acid to act efficiently as both proton acceptor and proton donor, an acidic pH similar to the pK_a of carboxylates is required, whereas histidine is efficient in this role at neutral pH. Acidic conditions ($\text{pH} \sim 3$) are optimal for CPO-catalyzed chlorination.¹⁶ It is postulated that at such low pH the redox potential of CPO-I is high enough to oxidize the chloride anion.¹⁷ Thus it is likely that CPO uses glutamic acid rather than histidine to facilitate the chlorinating function that gives

Received: March 22, 2012

Revised: September 12, 2012

Published: September 29, 2012



ACS Publications

© 2012 American Chemical Society

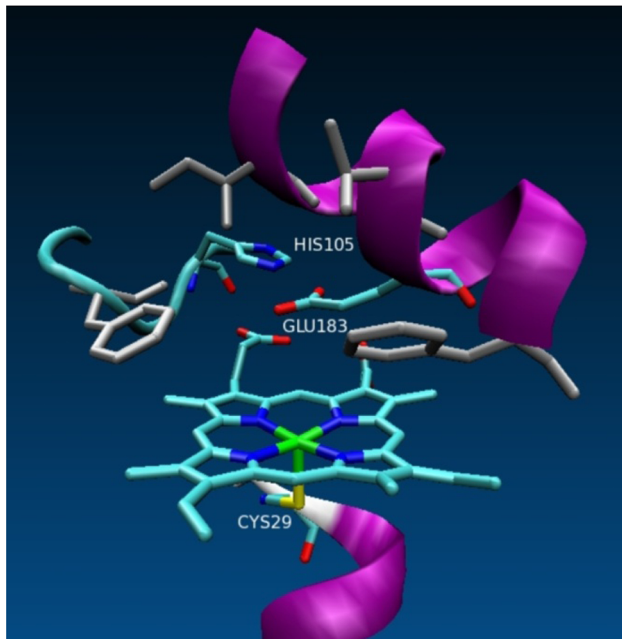


Figure 1. Hybrid features of X-ray structure of the active site of CPO.¹¹ Like P450, CPO's proximal pocket possesses a cysteine-derived thiolate ligand (Cys29). Like peroxidases, CPO's distal pocket possesses a polar residue with general acid–base properties (Glu183). Some of the hydrophobic residues of the distal pocket are shown in gray.

the enzyme its name.¹⁷ Traditional peroxidases acting at neutral pH cannot carry out chlorination.

The position and acid–base properties of the Glu183 carboxylate side chain are affected by hydrogen bonding with the imidazole side chain of His105 (Figure 1).^{11,15,18} Together, His105 and Glu183 have been referred to as a proton shuttle; the shuttle's role in catalyzing CPO-I formation is well established.^{19,20} The results of Glu183His²¹ mutation and His105²² alkylation suggest that these two residues affect not only Cpd I formation but also CPO-catalyzed oxidations. In addition to His105 and Glu183, the distal pocket contains a set of hydrophobic residues surrounding the active center.^{11,23} This hydrophobic core of residues constitutes most of the steric environment of the active center and is probably the primary cause of the stereoselectivity of oxidations carried out by CPO.^{11,22,23}

The hybrid peroxidase-P450 nature of CPO's active site is further manifested by access to the heme moiety. P450s have a deep distal pocket that enables substrate binding directly adjacent to the heme center, whereas the heme edge is not accessible.²⁴ In peroxidases, access to the heme center is limited, and substrates undergo electron-transfer reactions at the heme edge.²⁵ The heme moiety of CPO can be accessed through two channels, one narrow and one wide.²⁶ The wide channel connects the distal pocket to the enzyme surface, providing direct access to the heme center, whereas the narrow channel connects the heme edge to the surface. The crystal structures studied in ref 26 suggest that halides, which form hypohalite intermediates by reaction with CPO-I, may access the heme via the narrow channel.²⁶ It has also been established that one-electron, peroxidase-type oxidations generally occur at the surface of CPO, whereas the two-electron, P450-type stereoselective oxidations occur within the distal pocket of the enzyme.²²

Among CPO-catalyzed two-electron oxidations, the enantioselective epoxidation of olefinic substrates^{27–30} has attracted much attention in recent years, as chiral epoxides are useful synthons for many practical purposes.^{31–33} The mechanism of epoxidation of olefinic substrates by model Cpd I systems has been studied intensively using density functional theory (DFT).^{34–37} For these systems, which generally consist of the heme, a proximal thiolate ligand, the substrate, and possibly a few other moieties, it has been found that (i) the reaction proceeds in a stepwise manner, with formation of a single C–O bond followed by C–O–C ring closure to produce the epoxide;^{34–37} (ii) the initial C–O bond formation step is rate determining;^{34–37} (iii) the reaction rate correlates with the energy of the olefin π -bond;³⁷ (iv) the reaction is characterized by a “multi-state reactivity”, i.e., reaction can proceed on nearly degenerate low- and high-spin pathways, each offering subpathways characterized by subtly different electromer states;^{34–37} (v) the low-spin pathway is characterized by a barrierless C–O–C ring closure and preferentially forms the epoxide;^{34–37} (vi) the high-spin pathway possesses a barrier for ring closure, and the resulting radical intermediate may lead to side products or inversion of chirality.^{34–37} The olefin epoxidation reaction mechanisms could be further complicated by the possibility of spin-forbidden transitions due to spin–orbit coupling interactions³⁸ (see, for example, studies of methane³⁹ and ethane⁴⁰ C–H bond activation by FeO^+). It is thought that the kinetics of olefin epoxidation by Cpd I could be affected by spin-forbidden transitions at a crossing point of low- and high-spin surfaces at an intermediate stage of the reaction.^{34,35}

Despite this wealth of knowledge concerning model Cpd I systems, the influence of the CPO environment, in particular the distal pocket, on the mechanism of the epoxidation reaction has hardly been explored. Elucidating the nature of this influence is expected to yield understanding of CPO's catalytic versatility^{11,14,22} and of the enantiospecificity of the epoxidation reaction.^{11,22,23} The ability of CPO to catalyze many P450-type reactions⁷ implies that such a result could also further our understanding of the catalytic functions of P450s, which participate in key biochemical processes in many living species.⁴¹

The role of the distal pocket environment in CPO-catalyzed epoxidation of an olefinic substrate, *cis*- β -methylstyrene (CBMS), is the focus of this paper. CPO-catalyzed epoxidation of CBMS is of potential interest for pharmaceutical applications¹⁰ and has been the subject of a number of studies.^{10,17,23,27} CBMS is converted by CPO-I into 1S2R and 1R2S epoxides with a 96:4 ratio.²⁷ Thus it is a system of choice for understanding the source of CPO's epoxidation enantiospecificity. Presumably the high enantiomeric excess of the reaction is a result of distal pocket interactions with CBMS on the 1S2R and 1R2S reaction pathways. Sundaramoorthy et al. used early classical molecular mechanics (MM) methods to simulate a CPO-I/CBMS complex at the binding stage of the reaction.¹⁷ Based on the resemblance of X-ray structures of the resting state¹¹ and of CPO complexed with small ligands observed over a wide range of pH,¹⁷ they postulated that CPO catalysis does not require significant active site flexibility.¹⁷ Consequently they treated the protein backbone as a rigid replica of the resting state X-ray structure for their MD simulation.¹⁷ A similar approach was used recently in quantum mechanical/molecular mechanical studies of Cpd I²⁰ and Compound 0⁴² (the ferric hydroperoxide complex) forms of

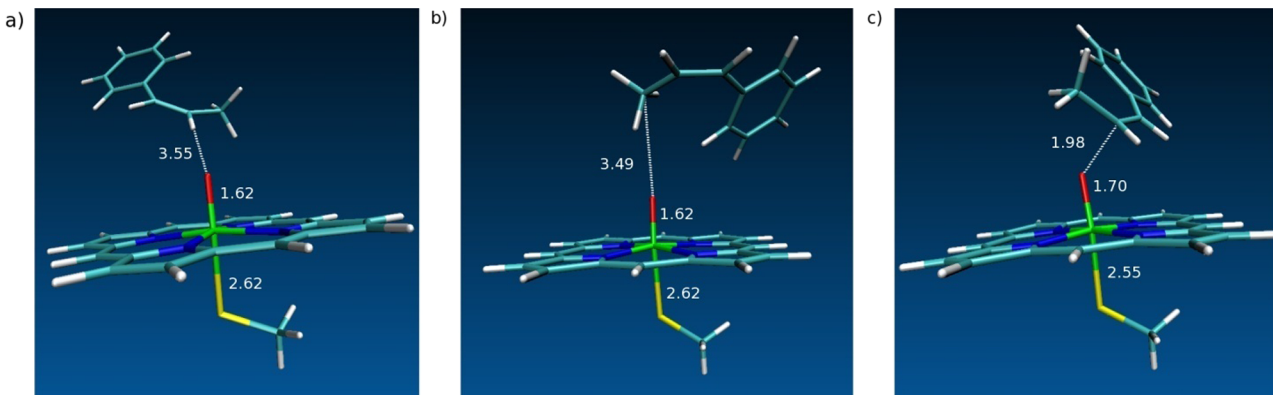


Figure 2. Optimized structures (doublet surface) of model Cpd I interacting with CBMS: (a) binding complex A; (b) binding complex B; (c) 1S2R transition state. Distances (\AA) of the Fe–S and Fe–O bonds are given in all three panels. In panels a and c, the remaining interatomic distance is for the O–C $_{\beta}$ atom pair; in panel b it is for the O–C atom pair, where C is the CBMS methyl carbon.

CPO. Mechanistic inflexibility of CPO's active site was also assumed in conceptualizing some experimental results regarding the enzyme's chlorination function.¹⁶

However, the rigid active site model may be unrealistic in the case of epoxidation. In a recent modeling study of the CPO-I/CBMS binding complex without the rigid active site restriction,²³ it was found that accommodating CBMS into a binding well is paralleled by a substantial displacement of the Glu183 side chain.²³ This is in line with a Glu183His mutant experimental study indicating that a distortion of the His105-Glu183 proton shuttle favors epoxidation over other catalytic reactions.²¹ These results led to the intuitively attractive postulate^{21,23} that the epoxidation activity of CPO requires distal pocket flexibility so that the native polar, peroxidase-like environment of the active center can be changed into the hydrophobic environment characteristic of P450. In previous work, we demonstrated that the enantiospecificity of the epoxidation reaction is not correlated with the relative favorability of particular prechiral binding complexes but is likely to be correlated with the effect of the distal pocket on the transition state.²³ To complete the assessment of the distal pocket's effect on the reaction barrier, extensive conformational sampling of the transition state modeled with the entire enzyme flexible is required.

Here we present a theoretical study of CPO-catalyzed epoxidation of CBMS with the aim of identifying key structural characteristics of the transition state for the rate-determining step,^{34–37} formation of the C $_{\beta}$ –O bond (C $_{\beta}$ and O denote the methyl-substituted olefinic carbon and the ferryl oxygen, respectively). The study is focused on the main reaction channel, the 1S2R enantiomeric pathway²⁷ on the doublet spin surface.^{34–37} The distal pocket effects were considered perturbations of a high energy gas phase transition state. Accordingly, the gas phase properties of a model (vide infra) Cpd I/CBMS transition state (TS) were found using DFT calculations. Following the Q2MM method,⁴³ an MM model of the TS state was created and docked into the distal pocket. The resulting CPO/TS complex was simulated using classical molecular dynamics (MD). Polar, steric, and hydrophobic effects of the distal pocket on the TS and the binding complex were determined using DFT and MM methods.

The major finding presented here is that the distal pocket environment enhances the inherent catalytic effect of a model, gas-phase Cpd I-like species, decreasing the 14 kcal/mol gas phase reaction barrier for epoxidation of CBMS by \sim 4 kcal/mol.

The reaction barrier lowering results from breathing of the distal pocket, which is enlarged during the binding stage and subsequently reduced in size to snugly fit the transition state. Simultaneously, the Glu183 side chain swings away from its resting state position in close proximity to the heme center, clearing a path for substrate approach to the ferryl oxygen. This displacement is promoted by a rearrangement of the Glu183 side chain interactions within the distal pocket. Together, breathing of the distal pocket and Glu183 displacement change the immediate environment of the active oxyferryl group from polar, peroxidase-like to hydrophobic, P450-like, thereby promoting approach of the nonpolar substrate and reducing the reaction barrier. This picture constitutes a new understanding of CPO's catalytic versatility. The distal pocket's flexibility allows the catalytic properties of CPO to be tuned by adjustment of the immediate environment of the oxyferryl group.

II. METHODS

Gas Phase DFT Calculations. Unrestricted DFT calculations of the doublet and quartet spin surfaces of 1S2R epoxidation were carried out using the B3LYP^{44,45} hybrid density functional with the LANL2DZ ECP double- ζ basis set for Fe⁴⁶ and the 6-31G* basis set for H, C, N, O,⁴⁷ and S⁴⁸ atoms.

This level of theory is currently accepted for modeling Cpd I electronic properties.^{34–37,49} The 43-atom model Cpd I species contained an oxyferryl moiety embedded in a porphyrin ring without side chains and with the cysteinate proximal ligand replaced by SCH₃⁻; thus, the active site of CPO-I was mimicked by the neutral species Fe⁴⁺O²⁻(N₄C₂₀H₁₂)⁻(SCH₃)⁻ (Figure 2). All calculations were performed without symmetry restrictions. The NWChem 6.0⁵⁰ molecular simulation package was used for geometry optimizations. The Gaussian 09⁵¹ electronic structure modeling package was used for stability checks of the optimized structures. Only stable structures were the subject of numerical normal-mode analysis using NWChem 6.0. All reported transition state structures had one vibrational mode with a negative eigenvalue. Optimized structures of binding complexes, intermediates, and epoxide products had positive eigenvalues only.

A variety of dispersion correction methods have recently been developed⁵² to overcome a deficiency in standard DFT, and we considered their use. However, Sherril et al.⁵² warned against using any dispersion correction as a "black box" for

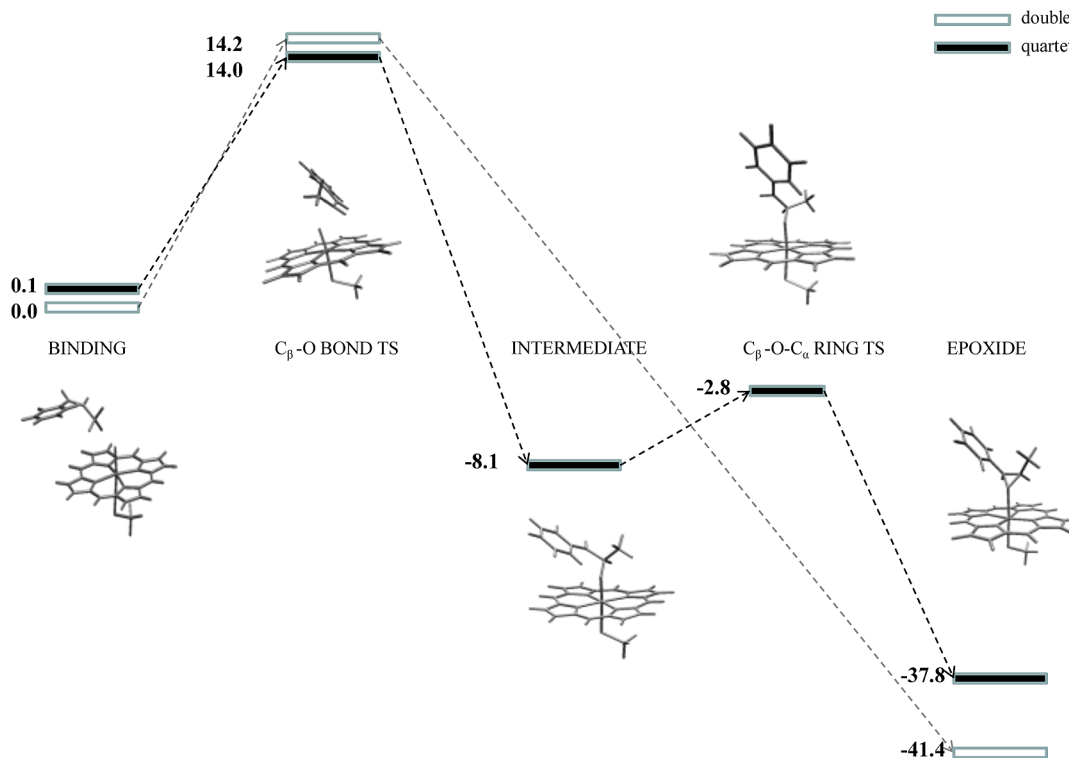


Figure 3. Doublet and quartet potential energy surfaces for 1S2R gas phase CBMS epoxidation by model Cpd I.

biomolecules. In particular they found that the accuracy of Grimme's type of corrections⁵³ deteriorates significantly if a basis set used for geometry optimization is not large enough.⁵² The NWChem 6.0 package has implemented Grimme's D2 dispersion correction,⁵⁴ and so the D2 correction in combination with B3LYP/6-31G*/LANL2DZ_ECP was calculated for the system of interest here. The results obtained were artificial, as inclusion of the D2 correction made the epoxidation reaction barrierless. Currently the B3LYP/6-31G*/LANL2DZ_ECP level of theory is well established in general for modeling Fe containing systems,⁵⁵ and in particular for modeling Cpd I properties^{34–37,49} so as described above, that is the method applied here.

MD Simulations. MD simulations were carried out with the biomolecular simulation program CHARMM,⁵⁶ using the CHARMM22 force field⁵⁷ including CMAP corrections.⁵⁸ Molecular mechanics parameters specific for CPO-I are given in ref 23. An all-atom MM force field for the TS⁵⁹ was developed using the Q2MM method.⁴³ The Q2MM method allows extensive conformational sampling of transition state/enzyme complexes and is especially suitable for modeling stereoselective enzyme catalysis.⁴³ It should be noted, however, that this method cannot yield absolute activation energies; only barrier differences can be calculated. In brief, this method modifies a quantum mechanical (QM) Hessian for a transition state structure by reversing the negative normal mode into a positive one; that is, the imaginary frequency is changed to a positive real value while the corresponding eigenvector remains the same. An MM model is then developed to reproduce the structure of the transition state and the normal modes of the modified QM Hessian. Effectively, barrier crossing motions for such an MM model are harmonically constrained to remain in the vicinity of the transition state, which becomes a regular energy minimum in the MM representation.⁴³ Consequently, a

plethora of modern MM methods becomes available for transition state simulations.

A model MM transition state was built that included the reacting CBMS, a bare oxyferryl heme without porphyrin side chains, and a proximal methyl thiolate ligand (the same system as in the QM model described above). At the beginning of the MM force field optimization, the reversal of the negative normal mode into a positive one was achieved by adding a C_β-O bond term to the MM model. The initial length of this bond was taken equal to the C_β-O distance in the TS, and the initial value of the corresponding force constant was that of a typical single C–O bond in the CHARMM22 force field.⁵⁷ Overall optimization of the MM transition state model was then carried out following the iterative procedure⁶⁰ recommended by Mackerel's group for developing CHARMM-compatible force fields. To optimize the normal modes, a scoring function was developed to estimate the difference between the modified QM and MM transition state Hessians. The MM normal modes were then optimized following the gradient of the scoring function in the space of force constant parameters. A detailed description of the optimization procedure for the MM model, along with the parameters developed, is given in the Supporting Information A (hereafter SI).

An initial structure for the CPO/TS complex was created by manually docking the TS into a CPO scaffold with the heme moiety removed. A 1S2R reaction precursor structure obtained in our previous MD study²³ was used to create the scaffold. After docking the TS, the CPO/TS structure was solvated in a truncated octahedral box of about 7000 TIP3P⁶¹ water molecules as modified for the CHARMM force field.⁵⁷ The protonation states of the titrable amino acid residues were assigned as follows: +1 for His, Lys; -1 for Glu, Asp; and neutral for Tyr. These values are appropriate for the optimal epoxidation activity of CPO characterized by pH values ranging

Table 1. Group Spin Densities (ρ) and Bond Lengths (Å) of Optimized Structures

| | | ρ_{SCH_3} | ρ_{por} | ρ_{Fe} | ρ_{O} | $\rho_{\text{C}\beta\text{H}}$ | ρ_{CatH} | ρ_{R1}^a | ρ_{R2}^a | S–Fe | Fe–O | $\text{O}-\text{C}_{\beta}$ | $\text{O}-\text{C}_{\alpha}$ |
|---|----------------|-----------------------|---------------------|--------------------|-------------------|--------------------------------|----------------------|----------------------|----------------------|-------|-------|-----------------------------|------------------------------|
| binding B | D ^b | -0.8 | -0.3 | 1.2 | 0.9 | 0.0 | 0.0 | 0.0 | 0.0 | 2.619 | 1.623 | 4.297 | 4.737 |
| | Q ^b | 0.75 | 0.25 | 1.1 | 0.9 | 0.0 | 0.0 | 0.0 | 0.0 | 2.622 | 1.624 | 4.321 | 4.818 |
| $\text{C}_{\beta}-\text{O}$ TS ^c | D | -0.7 | -0.35 | 1.0 | 0.75 | -0.15 | 0.4 | 0.05 | 0.00 | 2.554 | 1.705 | 1.985 | 2.634 |
| | Q | 0.6 | 0.15 | 1.05 | 0.8 | -0.1 | 0.4 | 0.1 | 0.0 | 2.458 | 1.698 | 1.979 | 2.697 |
| intermediate | D ^d | -0.45 | -0.35 | 1.0 | 0.2 | 0.0 | 0.4 | 0.2 | 0.0 | 2.447 | 1.839 | 1.501 | 2.208 |
| | Q | 0.1 | -0.1 | 1.65 | 0.3 | -0.05 | 0.8 | 0.25 | 0.05 | 2.309 | 1.805 | 1.414 | 2.432 |
| $\text{C}_{\beta}-\text{O}-\text{C}_{\alpha}$ TS ^c | Q | 0.3 | -0.1 | 2.20 | -0.05 | 0.0 | 0.5 | 0.15 | 0.0 | 2.399 | 1.952 | 1.408 | 2.154 |
| | D | 0.0 | 0.0 | 1.0 | 0.0 | 0.0 | 0.0 | 0.0 | 0.0 | 2.222 | 2.278 | 1.447 | 1.443 |
| epoxide | Q | 0.5 | 0.0 | 2.5 | 0.0 | 0.0 | 0.0 | 0.0 | 0.0 | 2.427 | 2.785 | 1.440 | 1.437 |

^aR1, benzylic group of CBMS; R2, methyl group of CBMS. ^bD, doublet; Q, quartet. ^c $\text{C}_{\beta}-\text{O}$ TS, TS leading to bond formation; $\text{C}_{\beta}-\text{O}-\text{C}$ TS, TS leading to ring closure. ^dThere is no stable intermediate on the doublet pathway. The structure with the smallest gradient was chosen instead.

from 4 to 6.⁶² The structure was neutralized by adding sodium cations, minimized, heated, and equilibrated to generate initial conditions for the MD simulation. For NPT dynamics, an extended system constant pressure and temperature algorithm⁶³ was chosen for keeping the pressure at 1 atm and the temperature at 298 K. The dynamics was propagated with the Verlet leapfrog algorithm using a time step of 1 fs. Coulomb interactions were calculated using the particle-mesh Ewald method,⁶⁴ with a cutoff of 10 Å for real-space interactions and a 1 Å grid with sixth-order B-spline interpolation for reciprocal-space interactions. Lennard-Jones forces were treated with the force switch method with a switching range of 8–10 Å. The SHAKE algorithm⁶⁵ was applied to constrain the lengths of all bonds involving hydrogens with allowed relative deviations of 10^{-10} .

III. RESULTS AND DISCUSSION

Cpd I/CBMS Gas Phase DFT Calculations. The saddle points leading to formation of the $\text{C}_{\beta}-\text{O}$ bond on the doublet and quartet pathways were found by scanning the $\text{C}_{\beta}-\text{O}$ distance followed by optimization to the saddle point. A 1S2R reaction precursor structure obtained in our previous MD study²³ was used as the starting point. The optimized TS structure on the doublet pathway is shown in Figure 2c. The doublet and quartet Cpd I/CBMS binding complexes were obtained by following the negative normal mode in the direction of increasing $\text{C}_{\beta}-\text{O}$ distance. The optimized Cpd I/CBMS binding complex structure on the doublet pathway (Figure 2b) is characterized by the steric interaction of the substrate methyl group with the ferryl oxygen. This type of 1S2R binding complex was found in our previous MD study and is shown as binding minimum B in Figure 4 of ref 23. In that study another 1S2R binding well was also found, binding minimum A shown in the same figure. This type of binding complex is characterized by the steric interaction of the substrate beta-carbon and the ferryl oxygen. Although in the CPO environment binding minima A and B are equivalent in free energy terms,²³ the DFT optimization of a model counterpart of minimum A results in the metastable structure shown in Figure 2a. This structure is 0.8 kcal/mol higher in energy than the structure in Figure 2b. Hereafter we use the capital letters A and B to denote these types of binding interactions, in correspondence with ref 23.

The intermediates with the beta-carbon covalently bound to the ferryl oxygen and the $\text{C}_{\alpha}-\text{O}-\text{C}_{\beta}$ ring opened (Figure 3) were sought by following the negative normal mode of the transition state preceding formation of the $\text{C}_{\beta}-\text{O}$ bond in the direction of decreasing $\text{C}_{\beta}-\text{O}$ distance. In agreement with

previous studies^{34–37} the doublet pathway connects the TS and the product complex in an effectively concerted manner without a barrier for $\text{C}_{\alpha}-\text{O}-\text{C}_{\beta}$ ring closure. The quartet pathway leads to an intermediate that is separated from the product complex by a relatively shallow barrier of 5.3 kcal/mol for $\text{C}_{\alpha}-\text{O}-\text{C}_{\beta}$ ring closure. The corresponding transition state was located by scanning the $\text{C}_{\alpha}-\text{O}$ distance followed by optimization to the saddle point. Finally, the epoxide products were found by relaxing the structures with the $\text{C}_{\alpha}-\text{O}-\text{C}_{\beta}$ ring closed.

Group spin densities and important bond lengths for the reported structures are summarized in Table 1. In agreement with previous studies,^{34–37} the intermediate with the lowest energy on the quartet pathway is an electromer characterized by a radical localized on the C_{α} position and by the iron having a +4 oxidation state (the spin density on the iron is close to two). On the doublet pathway, the radical electromer competes with electromers characterized by an additional delocalization of electron density from the C_{α} radical center to one of the Cpd I π^* orbitals made up of antibonding combinations of iron 3d and oxygen 2p atomic orbitals³⁶ (see Figure 2 of ref 36 for corresponding details of orbital occupancy). These types of electromers are referred as cationic,³⁶ and the iron is in a +3 oxidation state (the spin density on the iron is close to unity) once the transition state leading to $\text{C}_{\beta}-\text{O}$ bond formation is crossed. We found that on the doublet pathway the cationic electromer has the lowest energy for CBMS, while in the case of styrene the radical electromer was reported to be stable.³⁶

The doublet and quartet potential energy surfaces including zero-point energy corrections are shown in Figure 3. The rate-determining barriers for epoxidation are 14.2 and 13.9 kcal/mol on the doublet and quartet surfaces, respectively, relative to the nearly degenerate bound complexes. In line with previously published PESs for epoxidation of various olefinic substrates,^{34–37} our result shows that the doublet and quartet reaction pathways are close in energy. Previous studies^{35,36} showed that the relative order of the low- and high-spin pathways on the different stages of the olefin epoxidation reaction is sensitive to the nature of the substrate and to effects imposed by an enzyme environment. According to these studies, enzyme effects represented as model hydrogen bonds to the proximal thiolate ligand and/or model dielectric continuum solvation show a tendency to prefer the low-spin pathway for the rate determining $\text{C}_{\beta}-\text{O}$ bond formation. Given this tendency and the observation that the high-spin pathway is likely to lead to side products, we assumed, in agreement with the results in refs 34–37, that the low-spin pathway is the main channel for the epoxidation reaction.

To assess the catalytic rate enhancement due to Cpd I, we compared these barrier heights with the barrier for uncatalyzed epoxidation directly by hydrogen peroxide. We carried out calculations of the gas phase epoxidation of CBMS by hydrogen peroxide using DFT (SI B) and obtained a reaction barrier of 28.7 kcal/mol for the stepwise biradical mechanism.^{66,67} Thus, without accounting for the effect of the enzyme's environment, the bare Cpd I (the oxyferryl heme-thiolate moiety) reduces the reaction barrier for epoxidation of CBMS by 14.5 kcal/mol relative to uncatalyzed epoxidation.

MD Simulation of the TS. Because of the C_4 rotational symmetry of a pure porphyrin ring, each of the DFT-optimized structures has three counterparts that are nearly degenerate in energy but differ in the relative orientation of the proximal and distal iron substituents. The four structures have C_β -O-S- C_s dihedral angles spaced approximately 90° apart (C_s denotes the carbon of the sulfur methyl group). The MM models of these four TS conformers were considered for docking into CPO. The positions of the thiolate ligand and heme moiety relative to the scaffold are predetermined by the protein backbone connectivity and steric limitations of the active site pocket. For this reason three of the four possible CPO/TS conformations were unrealistic because of significant steric overlap between CBMS and the distal pocket residues. The remaining, realistic conformation was minimized over the TS degrees of freedom while keeping the CPO scaffold fixed. The resulting CPO/TS structure is shown in Figure 4. This

depicts the corresponding results²³ for the CPO-I/CBMS binding complexes A and B.

Breathing of the Distal Pocket. The distal pocket exhibits a mechanical opening-and-closing-like behavior during the CPO-I → CPO-I/CBMS → CPO/TS transitions. This behavior was revealed in several ways. The first is analysis of the distances between the active site center and the backbone of residues lining the distal pocket. Figure 6 presents interatomic distances for the residues in Figure 5 and for His105 for the CPO-I/CBMS A and B binding complexes²³ and for the TS relative to the corresponding values for CPO-I. The data are C_α -Fe distances for hydrophobic/neutral residues, and O(N)-Fe distances for the closest side chain atoms of charged residues Glu183 and His105, respectively. All data were averaged over the 20 ns MD simulations. The data show that the distal pocket "breathes", that is, it expands during the binding stage of the reaction and contracts during C_β -O bond formation.

Further insight into the distal pocket mechanical behavior was gained through analysis of the volume and the Lee-Richards accessible surface area (ASA)⁶⁸ of the distal pocket. The volume values for structures averaged over the trajectories were calculated using Voronoi tessellation as implemented in FPOCKET.⁶⁹ The Lee-Richards ASA values were calculated with a probe radius 1.4 Å and averaged over the simulated trajectories using CHARMM.⁵⁶ The trends in the volume and ASA (Table 2) of the distal pocket cavity confirm the distal pocket breathing. The cavity shrinks slightly when CPO-I is formed, increases in size during substrate binding, and returns to its resting-state size as the transition state is formed. The large differences in the volume between CPO-I, CPO-I/CBMS, and CPO/TS are due to expansion of the alpha helices lining the distal pocket and also to the conformational change of the C-terminal loop (Figure 7). The C-terminal loop is a loose secondary element of CPO's tertiary structure which to some degree serves as a lid to the distal pocket cavity. Upon substrate binding, the C-terminal loop makes steric contact with the substrate²³ and undergoes a relatively large displacement (Figure 7, SI D) which contributes to the differences observed in the cavity volume. The ASA parallels the volume change. Furthermore, the ASA of the substrate decreases from 27 (23) Å² for the CPO-I/CBMS A (B) complex to only 4 Å² for the CPO/TS complex (data not shown). Thus the contraction of the distal pocket at the TS stage of the reaction is accompanied by a nearly perfect burying of the substrate into the distal pocket cavity (the gas phase ASA of CBMS is 345 Å²).

Our result shows that breathing of the distal pocket involves a correlated behavior of the alpha helices lining the distal pocket and of the C-terminal loop (Figure 7). Similar mechanical behavior of secondary structure motifs was reported previously for P450⁷⁰ and cytochrome *c*.^{71,72} Principal component analysis (PCA)⁷³ was conducted to determine whether low frequency enzyme vibrational modes could be responsible for breathing. For the simulated trajectories the low frequency motions involving the distal pocket residues (for example Phe103) were found. However, for the available simulation times (20 ns), no low frequency motions were observed which can be unambiguously described as a correlated expansion and contraction of alpha carbons lining the distal pocket. It seems that breathing of the distal pocket is a ligand binding/escaping induced phenomenon. A long time dynamics simulation containing multiple events of binding and escaping of the substrate is necessary to definitively determine whether breathing of the distal pocket can be attributed to a low

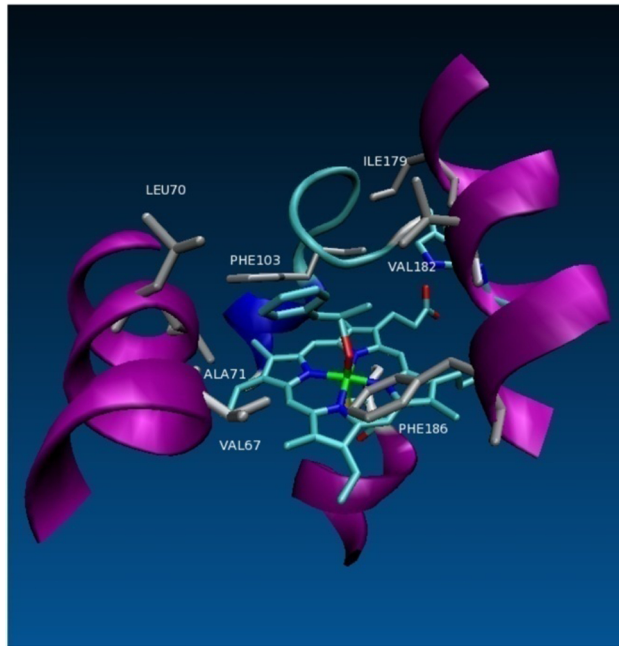


Figure 4. TS docked into the CPO scaffold. Hydrophobic residues in the distal pocket are shown in gray.

structure was used to initiate a 20 ns MD trajectory. The distal pocket residues interacting with the TS moiety were identified by calculating the probabilities of CPO/TS steric contacts averaged over the simulation trajectory. A steric contact was defined as a positive van der Waals energy for at least one residue/TS atom pair among all such pairs for a given residue. The result (Figure 5) establishes the sterically significant distal pocket environment of the TS. Figure 5 also

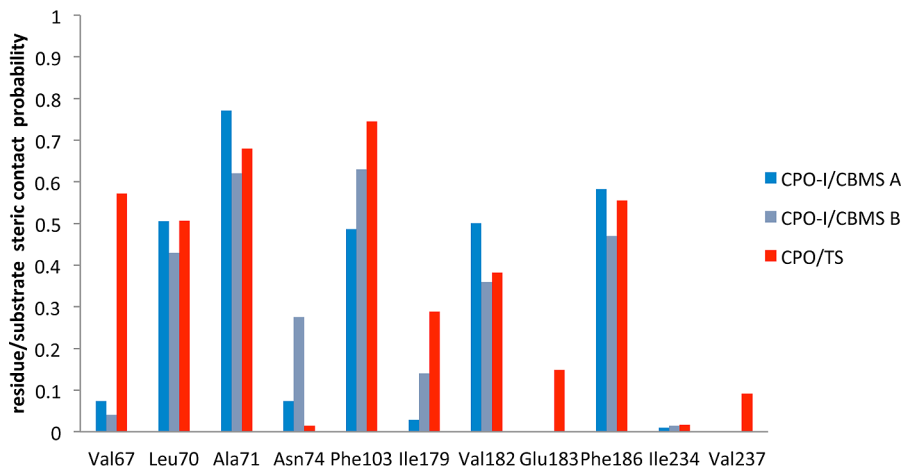


Figure 5. Histogram of probabilities for distal pocket residue/TS steric contacts.

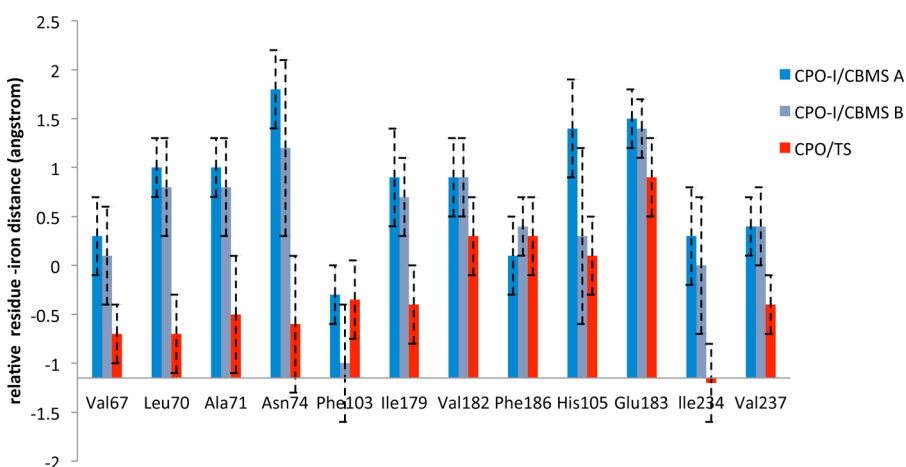


Figure 6. Breathing of the distal pocket demonstrated with selected interatomic distances for the CPO-I/CBMS A and B binding complexes²³ and for the TS relative to the corresponding values for CPO-I. The data are C_{α} -Fe distances for hydrophobic/neutral residues, and O(N)-Fe distances for the closest side chain atoms of Glu183(His105). The corresponding standard deviations are shown by dashed lines.

Table 2. Distal Pocket Cavity Volume of Average Structures for Selected States of CPO and Their ASA Averaged over Simulation Trajectories

| | X-ray ¹¹ | CPO-I | CPO-I/CBMS A ²³ | CPO-I/CBMS B ²³ | CPO/TS |
|------------------------|---------------------|-------|----------------------------|----------------------------|--------|
| volume/ \AA^3 | 390 | 260 | 730 | 620 | 380 |
| ASA/ \AA^2 | 360 | 297 | 416 | 391 | 370 |

frequency vibrational mode.⁷⁴ Such long simulations are beyond the scope of the work reported here.

In response to a referee's request, the observation of distal pocket expansion upon transformation of the binding complex into the TS was tested for hysteresis effects by reversing the transformation. To do this, the coordinates and velocities at the end of the TS simulation were used to start a "reversed" trajectory while the force field was changed back from one representing CPO/TS to one representing CPO-I/CBMS. In this "reversed" trajectory, transformation of the TS into the binding complex induced expansion of the distal pocket, in agreement with the results obtained for the forward simulations. A detailed account of the reversed trajectory is given in SI D.

Stabilization of the TS by the Hydrophobic Residues of the Distal Pocket.

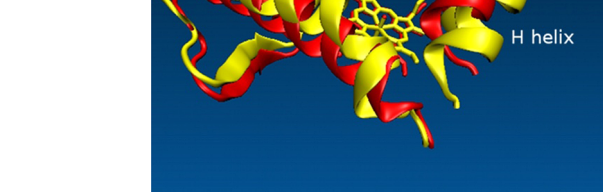


Figure 7. Breathing of the distal pocket revealed as a correlated behavior of the secondary structure elements. The averaged CPO structures for the TS and the substrate bound are shown in red and yellow, respectively. The nomenclature of the secondary structure elements is as given in ref 11.

the distal pocket are dominated by the hydrophobic residues (Figure 5). The enthalpic effect of the hydrophobic environment on the reaction barrier was estimated by averaging the

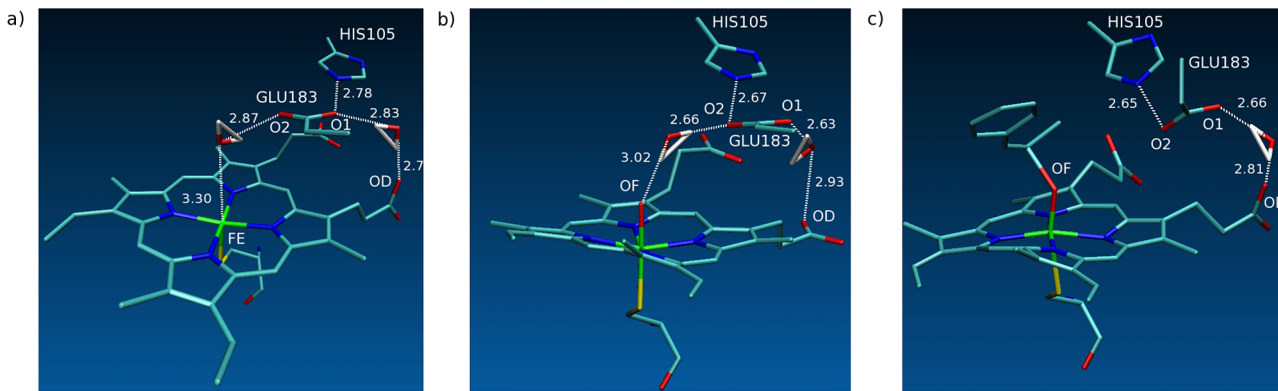


Figure 8. Interactions of the Glu183 side chain in (a) CPO X-ray structure;¹¹ (b) MD snapshot of CPO-I; (c) MD snapshot of CPO/TS complex. Important Glu183 interactions are shown by dashed lines with corresponding distances given in Å.

substrate's van der Waals interaction energies in the CPO-I/CBMS and CPO/TS complexes over the MD trajectories. The results are -15.9 (-15.3) and -19.4 kcal/mol for the CPO-I/CBMS A (B) and CPO/TS complexes, respectively. Thus, via the breathing mechanics, the distal pocket hydrophobic residues play a significant catalytic role in the CPO-catalyzed epoxidation of CBMS. This stabilization illustrates the modern paradigm for enzyme catalysis,⁷⁵ i.e., CPO stabilizes the transition state more than the bound substrate.

The enthalpic stabilization by hydrophobic residues of the distal pocket is supplemented by entropic stabilization arising from the hydrophobic effect,^{76,77} which can be estimated from the decrease in the ASA.⁷⁸ Averaged over the simulations, this effect corresponds to entropic stabilization by 1.3 (0.9) kcal/mol for the CPO-I/CBMS A (B) \rightarrow CPO/TS transition at ambient temperatures. Other significant entropic effects imposed by the enzyme environment could include vibrational entropy changes or a so-called "entropic stabilization" of the TS.⁷⁵ Full treatment of the entropic effects imposed by the enzyme environment is beyond the scope of this work and is planned as a separate study.

Effect of the Proton Shuttle on the TS. Although overall the His105-Glu183 proton shuttle is subject to breathing of the distal pocket, this alone is not sufficient to explain the mechanistic behavior of Glu183 during epoxidation. In the CPO/TS complex, which like the resting state has a small distal pocket volume (Table 2), the side chain of Glu183 is substantially displaced from its resting state position (Figure 6 and SI D). For the resting state, it was established previously that the close proximity of the Glu183 side chain to the active center is maintained by a set of specific interactions.¹¹ This set includes a water molecule bridging the heme iron and carboxylate oxygen O2 of Glu183 by forming hydrogen bonds with both, a hydrogen bond between nitrogen N2 of His105 and carboxylate oxygen O2 of Glu183, and another water molecule bridging carboxylate oxygen O1 of Glu183 and one of the heme propionates (atom nomenclature as per Figure 8).

This pattern of interactions was found to undergo a rearrangement in CPO-I and in the CPO-I/CBMS and CPO/TS complexes, as revealed by the corresponding probabilities averaged over MD simulations (Table 3). The water bridge between Glu183 O1 and the heme propionate is a permanent fixture across all these forms of the enzyme (probability of 1.0). For CPO-I without substrate present, the water bridging to Glu183 O2 maintains proximity to the ferryl

Table 3. Probabilities of Glu183 Side Chain Interactions during MD^a

| | CPO-I | CPO-I/CBMS A ²³ | CPO-I/CBMS B ²³ | CPO/TS |
|-------------|-------|----------------------------|----------------------------|--------|
| N2:O1 | 0.1 | 0.4 | 0.4 | 0.0 |
| N2:O2 | 0.9 | 0.6 | 0.5 | 0.9 |
| O2:water:OF | 1.0 | 0.0 | 0.0 | 0.0 |
| O1:water:OD | 1.0 | 1.0 | 1.0 | 1.0 |

^aAtom nomenclature is given in Figure 8.

oxygen rather than coordinating with the heme iron. This pushes the Glu183 side chain slightly away from the heme so that the His105 N2 hydrogen bonding preference changes from Glu183 O1 for the resting state to Glu183 O2 for CPO-I. The presence of the substrate fully displaces this water (bridging probability of 0.0) for both substrate-bound forms of CPO-I (A and B) and for the transition state, and causes the Glu183 side chain to swing away from the oxyferryl center (Figure 8).

The effect of displacement of the Glu183 side chain on the reaction barrier for epoxidation was assessed with single-point DFT calculations for the Cpd I/CBMS binding and TS structures (Figure 2) in the presence of the His105 and Glu183 side chains modeled as DFT-optimized $(\text{CH}_3\text{N}_2\text{C}_3\text{H}_4)^+$ and $(\text{CH}_3\text{CO}_2)^-$ moieties, respectively. Comparison was made with the barrier calculated without the His105-Glu183 pair present (Figure 3). With the His105-Glu183 side-chain pair in its average position during MD of the CPO/TS complex (colored side chains in Figure 9), a minor 0.5 kcal/mol reduction of the reaction barrier was observed. With the side-chain pair positioned as in the crystal-structure, resting-state conformation¹¹ (gray side chains in Figure 9), on the other hand, the reaction barrier is raised by ~ 30 kcal/mol (note that because it reflects single-point calculations, this number should be considered as qualitative indication rather than quantitative measure of the barrier destabilization). This destabilization is primarily due to interactions that the Glu183 side chain has with the transition state but not with the substrate in the binding complexes. These calculations reinforce the observation that the mobility of the Glu183 side chain is a critical structural prerequisite for the epoxidation reaction. Both the resting state conformer and the CPO/TS conformer of the Glu183 side chain are important for the full cycle of the epoxidation reaction; an inflexible active site model¹⁷ is not realistic in this case.

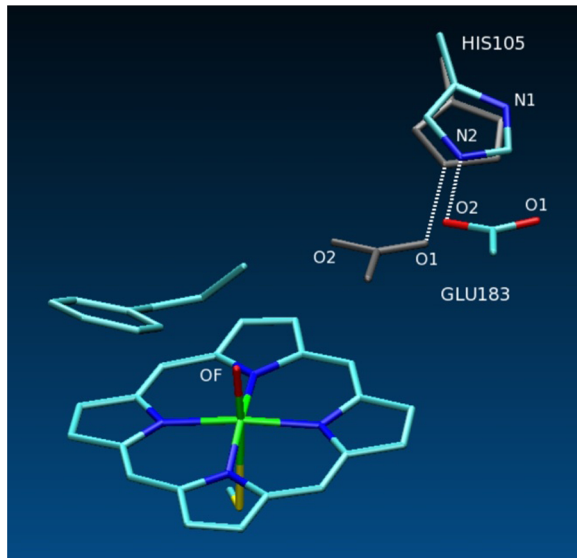


Figure 9. Structures used to calculate the effect of the Glu183 displacement on the TS for epoxidation (gray color indicates CPO resting state). The His105–Glu183 hydrogen bond is shown by dashed lines.

The overall picture emerging is that the position of the Glu183 side chain is tuned for each stage of the epoxidation reaction. In the resting state, Glu183 is positioned near the active site to assist with formation of CPO-I from the peroxide-bound complex. As CPO-I is formed, the Glu183 side chain moves slightly to allow formation of a water bridge with the ferryl oxygen but remains in close proximity to the oxyferryl center. It is likely that this water bridge stabilizes CPO-I and protects the enzyme from destructive autoxidation. (CPO was the first heme-thiolate enzyme for which the putative CPO-I species could be detected spectroscopically.^{5,79}) As the substrate approaches, the Glu183 side chain swings away from the active center, allowing the substrate to interact with the ferryl oxygen and rendering the distal pocket more hydrophobic. This picture provides a connection between two postulates concerning the active site, one based on X-ray crystallography and proposing a relatively inflexible active site¹⁷ and the other based on study of a Glu183His mutant and suggesting that a distortion of the His105-Glu183 proton shuttle favors epoxidation.²¹ These two postulates are patterned on different structural states of the distal pocket. The two sets of data are consistent within our proposed concept for the dynamical functioning of CPO's active site.

IV. CONCLUSION

This study demonstrates that the catalytic effect of Cpd I is tuned by flexibility of the distal pocket during CPO-catalyzed epoxidation of CBMS. The hydrophobic residues of the distal pocket significantly reduce the barrier for epoxidation. The structural basis for this is revealed as breathing of the distal pocket, as a result of which the enzyme stabilizes the transition state more than the bound substrate. The mobility of the Glu183 side chain within the distal pocket is found to be a prerequisite for epoxidation. This is because the Glu183 side chain has to be positioned near the active center to catalyze Cpd I formation and must subsequently be displaced as the olefinic substrate approaches the active center.

The mobility of the Glu183 side chain derives from rearrangement of an intricate set of interactions and enables the distal pocket to assume a more hydrophobic aspect or “face” during epoxidation and a more polar aspect or “face” during Cpd I formation, halogenation, and dismutation. It appears that the versatility of CPO's catalytic activity is enhanced by the distal pocket's ability to efficiently utilize its peroxidase-P450 hybrid construction and take on structurally different polar and hydrophobic faces. The metaphorical characterization of CPO as a Janus enzyme introduced by Hager et al.²² is therefore apt and derives from CPO's capacity to change its catalytic face by altering the structure of the distal pocket.

■ ASSOCIATED CONTENT

Supporting Information

MM force field parameters of the TS; hydrogen peroxide epoxidation of *cis*- β -methylstyrene: gas phase DFT calculations; absolute energies and Cartesian coordinates of the stationary points; reversed trajectory simulation and breathing of the distal pocket. This material is available free of charge via the Internet at <http://pubs.acs.org>.

■ AUTHOR INFORMATION

Corresponding Author

*E-mail: David.Chatfield@fiu.edu; omorozov@fiu.edu.

Notes

The authors declare no competing financial interest.

■ ACKNOWLEDGMENTS

The authors acknowledge Xiaotang Wang and Alexander M. Mebel for helpful discussions and comments. This work was supported by the NIH (SC3GM83723).

■ REFERENCES

- (1) Shaw, P. D.; Hager, L. P. *J. Am. Chem. Soc.* **1959**, *81*, 1011–1012.
- (2) Morris, D. R.; Hager, L. P. *J. Biol. Chem.* **1966**, *241*, 1763–1768.
- (3) Hager, L. P.; Morris, D. R.; Brown, F. S.; Eberwein, H. *J. Biol. Chem.* **1966**, *241*, 1769–1777.
- (4) Libby, R. D.; Beachy, T. M.; Phipps, A. K. *J. Biol. Chem.* **1996**, *271*, 21820–21827.
- (5) Rutter, R.; Hager, L. P. *J. Biol. Chem.* **1982**, *257*, 7958–7961.
- (6) Kim, S. H.; Perera, R.; Hager, L. P.; Dawson, J. H.; Hoffman, B. M. *J. Am. Chem. Soc.* **2006**, *128*, 5598–5599.
- (7) Dawson, J. H.; Sono, M. *Chem. Rev.* **1987**, *87*, 1255–1276.
- (8) Cedrone, F.; Ménez, A.; Quéméneur, E. *Curr. Opin. Struc. Biol.* **2000**, *10*, 405–410.
- (9) Shaw, P. D.; Hager, L. P. *J. Biol. Chem.* **1961**, *236*, 1626–1630.
- (10) Hager, L. P. *J. Biol. Chem.* **2010**, *285*, 14852–14860.
- (11) Sundaramoorthy, M.; Terner, J.; Poulos, T. L. *Structure* **1995**, *3*, 1367–1378.
- (12) Poulos, T. L. *J. Biol. Inorg. Chem.* **1996**, *1*, 356–359.
- (13) Dawson, J. H.; Holm, R. H.; Trudell, J. R.; Barth, G.; Linder, R. E.; Bunnenberg, E.; Djerassi, C.; Tang, S. C. *J. Am. Chem. Soc.* **1976**, *98*, 3707–3709.
- (14) Yi, X. W.; Mroczko, M.; Manoj, K. M.; Wang, X. T.; Hager, L. P. *Proc. Natl. Acad. Sci. U.S.A.* **1999**, *96*, 12412–12417.
- (15) Wang, X.; Tachikawa, H.; Yi, X.; Manoj, K. M.; Hager, L. P. *J. Biol. Chem.* **2003**, *278*, 7765–7774.
- (16) Manoj, K. M. *Biochim. Biophys. Acta* **2006**, *1764*, 1325–1339.
- (17) Sundaramoorthy, M.; Terner, J.; Poulos, T. L. *Chem. Biol.* **1998**, *5*, 461–473.
- (18) Blanke, S. R.; Hager, L. P. *J. Biol. Chem.* **1990**, *265*, 12454–12461.

- (19) Filizola, M.; Loew, G. H. *J. Am. Chem. Soc.* **2000**, *122*, 3599–3605.
- (20) Chen, H.; Hirao, H.; Derat, E.; Schlichting, I.; Shaik, S. *J. Phys. Chem. B* **2008**, *112*, 9490–9500.
- (21) Yi, X.; Conesa, A.; Punt, P. J.; Hager, L. P. *J. Biol. Chem.* **2003**, *278*, 13855–13859.
- (22) Manoj, K. M.; Hager, L. P. *Biochemistry* **2008**, *47*, 2997–3003.
- (23) Morozov, A. N.; D'Cunha, C.; Alvarez, C. A.; Chatfield, D. C. *Biophys. J.* **2011**, *100*, 1066–1075.
- (24) Poulos, T. L.; Finzel, B. C.; Howard, A. J. *J. Mol. Biol.* **1987**, *195*, 687–700.
- (25) Finzel, B. C.; Poulos, T. L.; Kraut, J. *J. Biol. Chem.* **1984**, *259*, 13027–13036.
- (26) Kuhnel, K.; Blankenfeldt, W.; Terner, J.; Schlichting, I. *J. Biol. Chem.* **2006**, *281*, 23990–23998.
- (27) Allain, E. J.; Hager, L. P.; Deng, L.; Jacobsen, E. N. *J. Am. Chem. Soc.* **1993**, *115*, 4415–4416.
- (28) Colonna, S.; Gaggero, N.; Casella, L.; Carrea, G.; Pasta, P. *Tetrahedron: Asymmetry* **1993**, *4*, 1325–1330.
- (29) Dexter, A. F.; Lakner, F. J.; Campbell, R. A.; Hager, L. P. *J. Am. Chem. Soc.* **1995**, *117*, 6412–6413.
- (30) Lakner, F. J.; Hager, L. P. *J. Org. Chem.* **1996**, *61*, 3923–3925.
- (31) Hager, L. P.; Lakner, F. J.; Basavapatruni, A. *J. Mol. Catal. B: Enzym.* **1998**, *5*, 95–101.
- (32) Tzialla, A. A.; Kalogeris, E.; Gournis, D.; Sanakis, Y.; Stamatis, H. *J. Mol. Catal. B: Enzym.* **2008**, *51*, 24–35.
- (33) Rai, G. P.; Flórez, A. M.; Hager, L. P. *Adv. Synth. Catal.* **2001**, *343*, 638–645.
- (34) de Visser, S. P.; Ogliaro, F.; Harris, N.; Shaik, S. *J. Am. Chem. Soc.* **2001**, *123*, 3037–3047.
- (35) de Visser, S. P.; Ogliaro, F.; Sharma, P. K.; Shaik, S. *J. Am. Chem. Soc.* **2002**, *124*, 11809–11826.
- (36) Kumar, D.; de Visser, S. P.; Shaik, S. *Chem.—Eur. J.* **2005**, *11*, 2825–2835.
- (37) Kumar, D.; Karamzadeh, B.; Sastry, G. N.; de Visser, S. P. *J. Am. Chem. Soc.* **2010**, *132*, 7656–7667.
- (38) Harvey, J. N. *Phys. Chem. Chem. Phys.* **2007**, *9*, 331–343.
- (39) Shiota, Y.; Yoshizawa, K. *J. Chem. Phys.* **2003**, *118*, 5872–5879.
- (40) Sun, X.-L.; Huang, X.-R.; Li, J.-L.; Huo, R.-P.; Sun, C.-C. *J. Phys. Chem. A* **2012**, *116*, 1475–1485.
- (41) Sono, M.; Roach, M. P.; Coulter, E. D.; Dawson, J. H. *Chem. Rev.* **1996**, *96*, 2841–2888.
- (42) Lai, W.; Chen, H.; Cho, K.-B.; Shaik, S. *J. Phys. Chem. A* **2009**, *113*, 11763–11771.
- (43) Norrby, P.-O. *J. Mol. Struct.: THEOCHEM* **2000**, *506*, 9–16.
- (44) Becke, A. D. *J. Chem. Phys.* **1993**, *98*, 5648–5652.
- (45) Lee, C.; Yang, W.; Parr, R. G. *Phys. Rev. B* **1988**, *37*, 785–789.
- (46) Hay, P. J.; Wadt, W. R. *J. Chem. Phys.* **1985**, *82*, 299–310.
- (47) Hariharan, P. C.; Pople, J. A. *Theor. Chim. Acta* **1973**, *28*, 213–222.
- (48) Franc, M. M.; Pietro, W. J.; Hehre, W. J.; Binkley, J. S.; Gordon, M. S.; DeFrees, D. J.; Pople, J. A. *J. Chem. Phys.* **1982**, *77*, 3654–3665.
- (49) Harris, D. L. *Curr. Opin. Chem. Biol.* **2001**, *5*, 724–735.
- (50) Valiev, M.; Bylaska, E. J.; Govind, N.; Kowalski, K.; Straatsma, T. P.; Van Dam, H. J. J.; Wang, D.; Nieplocha, J.; Apra, E.; Windus, T. L.; de Jong, W. A. *Comput. Phys. Commun.* **2010**, *181*, 1477–1489.
- (51) Frisch, M. J.; et al. *Gaussian 09*, revision A.1; Gaussian, Inc.: Wallingford, CT, 2009.
- (52) Burns, L. A.; Mayagoitia, A. V.; Sumpter, B. G.; Sherrill, C. D. *J. Chem. Phys.* **2011**, *134*, 084107.
- (53) Grimme, S.; Antony, J.; Ehrlich, S.; Krieg, H. *J. Chem. Phys.* **2010**, *132*, 154104.
- (54) Grimme, S. *J. Comput. Chem.* **2006**, *27*, 1787–1799.
- (55) Yang, Y.; Weaver, M. N.; Merz, K. M. *J. Phys. Chem. A* **2009**, *113*, 9843–9851.
- (56) Brooks, B. R.; et al. *J. Comput. Chem.* **2009**, *30*, 1545–1615.
- (57) MacKerell, A. D.; et al. *J. Phys. Chem. B* **1998**, *102*, 3586–3616.
- (58) MacKerell, A. D.; Feig, M.; Brooks, C. L. *J. Comput. Chem.* **2004**, *25*, 1400–1415.
- (59) Eksterowicz, J. E.; Houk, K. N. *Chem. Rev.* **1993**, *93*, 2439–2461.
- (60) Vanommeslaeghe, K.; Hatcher, E.; Acharya, C.; Kundu, S.; Zhong, S.; Shim, J.; Darian, E.; Guvench, O.; Lopes, P.; Vorobyov, I.; MacKerell, A. D. *J. Comput. Chem.* **2009**, *31*, 671–690.
- (61) Jorgensen, W. L.; Chandrasekhar, J.; Madura, J. D.; Impey, R. W.; Klein, M. L. *J. Chem. Phys.* **1983**, *79*, 926–935.
- (62) Manoj, K. M.; Hager, L. P. *Biochim. Biophys. Acta* **2001**, *1547*, 408–417.
- (63) Hoover, W. G. *Phys. Rev. A* **1985**, *31*, 1695–1697.
- (64) Essmann, U.; Perera, L.; Berkowitz, M. L.; Darden, T.; Lee, H.; Pedersen, L. G. *J. Chem. Phys.* **1995**, *103*, 8577–8593.
- (65) Ryckaert, J.-P.; Ciccotti, G.; Berendsen, H. J. C. *J. Comput. Phys.* **1977**, *23*, 327–341.
- (66) Freccero, M.; Gandolfi, R.; Sarzi-Amadè, M.; Rastelli, A. *J. Org. Chem.* **2002**, *68*, 811–823.
- (67) de Visser, S. P.; Kaneti, J.; Neumann, R.; Shaik, S. *J. Org. Chem.* **2003**, *68*, 2903–2912.
- (68) Lee, B.; Richards, F. M. *J. Mol. Biol.* **1971**, *55*, 379–400.
- (69) Le Guilloux, V.; Schmidtke, P.; Tuffery, P. *BMC Bioinformat.* **2009**, *10*, 168.
- (70) Paulsen, M. D.; Ornstein, R. L. *Proteins: Struct., Funct., Genet.* **1995**, *21*, 237–243.
- (71) Krishna, M. M. G.; Lin, Y.; Rumbley, J. N.; Englander, S. W. *J. Mol. Biol.* **2003**, *331*, 29–36.
- (72) Tsai, M. Y.; Morozov, A. N.; Chu, K. Y.; Lin, S. H. *Chem. Phys. Lett.* **2009**, *475*, 111–115.
- (73) Brooks, B. R.; Janežič, D.; Karplus, M. *J. Comput. Chem.* **1995**, *16*, 1522–1542.
- (74) Balsera, M. A.; Wriggers, W.; Oono, Y.; Schulten, K. *J. Phys. Chem.* **1996**, *100*, 2567–2572.
- (75) Garcia-Viloca, M.; Gao, J.; Karplus, M.; Truhlar, D. G. *Science* **2004**, *303*, 186–195.
- (76) Smith, D. E.; Zhang, L.; Haymet, A. D. *J. Am. Chem. Soc.* **1992**, *114*, 5875–5876.
- (77) Morozov, A. N.; Lin, S. H. *J. Chem. Phys.* **2009**, *130*, 074903.
- (78) Sharp, K. A.; Nicholls, A.; Fine, R. F.; Honig, B. *Science* **1991**, *252*, 106–109.
- (79) Rittle, J.; Green, M. T. *Science* **2010**, *330*, 933–937.